Compact beam splitters based on self-imaging phenomena in one-dimensional photonic crystal waveguides

Bing Chen (陈 兵)[1*], Lin Huang (黄 琳)[1], Yongdong Li (李永东)[1], Chunliang Liu (刘纯亮)[1], and Guizhong Liu (刘贵忠)[2]

[1] *Key Laboratory of Physical Electronics and Devices of the Ministry of Education, Xi'an Jiaotong University, Xi'an 710049, China*

[2] *Institute of Information and Communication Engineering, Xi'an Jiaotong University, Xi'an 710049, China*

[*] *Corresponding author: chenbing1975@hotmail.com*

Received March 26, 2012; accepted May 28, 2012; posted online September 14, 2012

A fundamental 1×2 beam splitter based on the self-imaging phenomena in multi-mode one-dimensional (1D) photonic crystal (PC) waveguides is presented, and its transmission characteristics are investigated using the finite-difference time-domain method. Calculated results indicate that a high transmittance (>95%) can be observed within a wide frequency band for the 1×2 beam splitter without complicated structural optimizations. In this letter, a simple and compact 1×4 beam splitter is constructed by combining the fundamental 1×2 beam splitter with the flexible bends of 1D PC waveguides. Such beam splitters can be applied to highly dense photonic integrated circuits.

OCIS codes: 130.5296, 230.1360, 130.3120.

doi: 10.3788/COL201210.111301.

Beam splitters are the most commonly used power division devices in the field of integrated optics. The development of highly dense photonic integrated circuits (ICs) has raised the need for compact beam splitters. A considerable number of compact beam splitters based on line and point defects in two-dimensional (2D) photonic crystals (PCs) have been presented and these can be approximately classified into the following three kinds according to their working mechanisms: T/Y branch[1−4], directional coupling[5−7], and multi-mode interference (MMI, or self-imaging phenomena) types[8−10]. T/Y branches are compact, but their branching angles are restricted by the lattice type of 2D PCs. Moreover, the branching regions of T/Y branches require complicated optimizations[1−4]. Devices based on waveguide coupler or MMI are much simpler than T/Y branches, but they tend to have a larger area (with a long coupling or beat length). Moreover, beam splitters based on 2D PCs are not flexible, i.e., the waveguide bends in the beam splitters are not only restricted by the lattice type of 2D PCs, but they also require special optimized designs[3,4,8,10]. The limitations above constrain the design and application of beam splitters based on 2D PCs.

Chen *et al.* have proposed a flexible waveguide (a one-dimensional (1D) PC waveguide) based on the omnidirectional reflection of 1D PCs[11,12]. This flexible waveguide can be bent arbitrarily with small radius of curvature, and its flexibility is similar to that of conducting wires in electronics. The same authors also proposed a power beam splitter for TE polarization based on the directional coupling of flexible waveguides[13]. Inspired by the ideas above, this letter proposes a fundamental 1×2 beam splitter for TE polarization based on the self-imaging phenomena in flexible waveguides. A simple and compact 1×4 beam splitter can be constructed when three fundamental 1×2 beam splitters are combined with the flexible bends of 1D PC waveguides.

In this letter, the beat lengths of self-imaging phenomena in multi-mode flexible waveguides are analyzed. Then, the fundamental 1×2 beam splitter based on the self-imaging phenomena in flexible waveguides is constructed, and its transmission characteristics are discussed. Then, a compact 1×4 beam splitter is constructed based on the combination of three fundamental 1×2 beam splitters, and its transmission characteristics are investigated.

The inset in Fig. 1(a) shows the schematic drawing of a flexible waveguide that consists of a dielectric layer with low index sandwiched by 1D PCs (X-axis direction), where a is the lattice constant of the 1D PCs, n_1=1.6 (polystyrene), n_2=4.6 (tellurium), and n_0=1 (air) are the refractive indices of the three materials, and h_1=0.75a, h_2=0.25a, and h_0 (defect channel) are the corresponding thicknesses. The light is defined in and along the defect channel (Z-axis direction) by the omnidirectional reflection band (ORB) from the 1D PCs, and β is the propagation constant. The waveguide is infinitely homogeneous along the Y-axis direction. The TE mode dispersion curves of the flexible waveguide with h_0=3.75a were calculated using the plane wave expansion method based on a super-cell[14], as shown in Fig. 1. The frequency range of the first photonic band-gap (PBG) of the 1D PCs in the case of normal incidence was 0.1450–

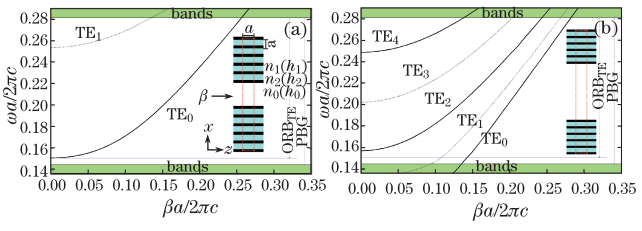

Fig. 1. (Color online) TE mode dispersion curves of the flexible waveguides with defect channel width of h_0=(a) 3.75a and (b) 9.75a. The schematic drawing of the flexible waveguide is shown in the inset, where a denotes the lattice constant of the 1D PC, n_1=1.6, n_2=4.6, n_0=1, h_1=0.75a, and h_2=0.25a.

0.2810 $[2\pi c/a]$ (c is the speed of light in vacuum), and the frequency range of the first ORB for TE mode (ORB_{TE}) was 0.1510–0.2810 $[2\pi c/a]$.

The numerical results show that the frequency range of TE_0 single mode (zero-order even mode) was 0.1511–0.2532 $[2\pi c/a]$ for the flexible waveguide with h_0=3.75a. Figure 1(b) shows the TE mode dispersion curves of the flexible waveguide with h_0=9.75a, where five dispersion curves corresponding to the TE_0, TE_1, TE_2, TE_3, and TE_4 modes, respectively, can be observed within the frequency range of ORB_{TE}.

As can be seen in Figs. 1(a) and (b), one mode (TE_0) and four modes (TE_0, TE_1, TE_2, and TE_3) correspond to the flexible waveguides with h_{01}=3.75a and h_{02}=9.75a (shown in Fig. 2), respectively, in the frequency range of 0.1572–0.2488 $[2\pi c/a]$. If the TE_0 mode in the flexible waveguide with h_{01}=3.75a within the 0.1572–0.2488 $[2\pi c/a]$ frequency range is regarded as an input field profile, both the TE_0 and TE_2 modes in the flexible waveguide with h_{02}=9.75a are stimulated (TE_1 and TE_3 modes in the flexible waveguide with h_{02}=9.75a cannot be stimulated), and the interference between the TE_0 and TE_2 modes leads to the self-imaging phenomena. Self-imaging is a property of multi-mode waveguides by which an input field profile is reproduced in single or multiple images at periodic intervals along the propagation axis[15]. If the first two-fold image distance is defined as L, then both the first single image distance and the beat length can be denoted as $2L$[15].

If the propagation constants of the TE_0 and TE_2 modes in the flexible waveguide with h_{02}=9.75a are denoted as β_0 and β_2, respectively, then L can be expressed as $\pi/(\beta_0$-$\beta_2)$. Figure 3 shows the calculated L based on Fig. 1(b), where L increased from 3.72a at the frequency of 0.158 $[2\pi c/a]$ to 10.89a at the frequency of 0.2487 $[2\pi c/a]$ with the increase in frequency due to the decrease in β_0-β_2.

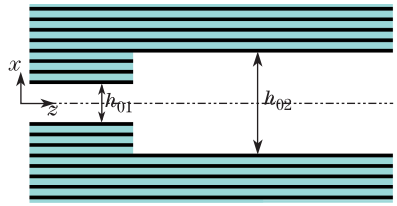

Fig. 2. Schematic drawing of the self-imaging phenomena in multi-mode flexible waveguides, where h_{01}=3.75a, h_{02}=9.75a, and the other parameters are the same as those in Fig. 1.

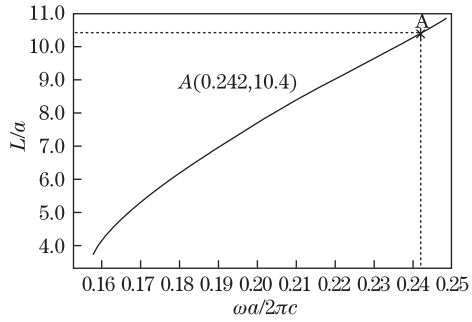

Fig. 3. The first two-fold image distance L of the self-imaging phenomena in the multimode flexible waveguide shown in Fig. 2 at the frequency range of 0.1572–0.2488 $[2\pi c/a]$.

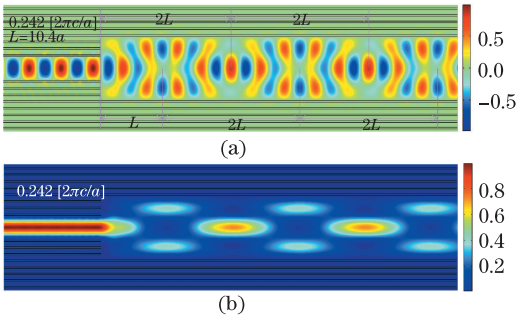

Fig. 4. (Color online) Self-imaging phenomena in the multi-mode flexible waveguide shown in Fig. 3. (a) Steady-state electric field E_y distribution and (b) time-averaged Poynting vector P_z distribution at the normalized frequency of 0.242 $[2\pi c/a]$. The first two-fold image distance is L, and both the first single image distance and the beat length are $2L$.

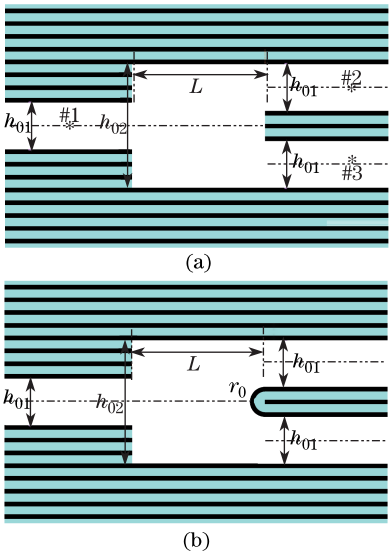

Fig. 5. (a) Schematic drawing of a 1×2 beam splitter with [h_{01}, h_{02}, L]=[3.75a, 9.75a, 10.4a] based on the self-imaging phenomena in multi-mode flexible waveguides. (b) Schematic drawing of an optimized 1×2 beam splitter, where $r_0 = a$ and the other parameters are the same as those cited above.

Figure 4 shows the self-imaging phenomena in the multi-mode flexible waveguide with h_{02}=9.75a. Figures 4(a) and (b) show the steady-state electric field E_y distribution and the time-averaged Poynting vector P_z distribution at the frequency 0.242 $[2\pi c/a]$ (denoted as A point in Fig. 3), respectively. The first two-fold image distance was defined as L(10.4a) and the first single image distance was $2L$(20.8a). An input field profile was reproduced in the single- and two-fold images at the periodic interval of $2L$ (the beat length) along the propagation axis (Z-axis direction).

Figure 5 shows a 1×2 beam splitter based on the self-imaging phenomena in flexible waveguides. As can be seen in Figs. 3 and 4, a 1×2 beam splitter with [h_{01}, h_{02}, L] = [3.75a, 9.75a, 10.4a] (corresponding to A points in Fig. 3) was constructed and its transmission characteristics were simulated using the finite-difference time-domain (FDTD) method[1,13,16]. In the numerical calculations, the perfectly matched layer-absorbing boundary conditions were applied to the four boundaries

of the computed region. The input pulse and the reflection pulse from the MMI region with [h_{02}, L]=[9.75a, 10.4a] in the time domain were picked up at observation point #1 in the middle of the input waveguide, whereas the two pulses transmitted through the MMI region were picked up at observation points #2 and #3 in the middle of the two output waveguides, respectively. Then, the reflection and transmission spectra were calculated from the Fourier transform of the time-domain pulses. A reflection spectrum and two transmission spectra were normalized using an input spectrum to obtain the normalized refection spectrum and transmission spectra, respectively. Finally, the sum of the normalized transmittances recorded at observation points #2 and #3 was defined as the total transmittance (denoted as T_t). If the calculation errors are omitted, the normalized transmission loss L_o can be expressed as L_o=1−T_t − F, where F is the normalized reflectance. A high transmittance band (HTB) is defined as the frequency band corresponding to $T_t \geqslant$0.95.

Figure 6(a) shows the transmission spectra, reflection spectrum, and loss spectrum of the 1×2 beam splitter with [h_{01}, h_{02}, L]=[3.75a, 9.75a, 10.4a] in Fig. 5(a). The transmittances at the two output ports exhibited good consistencies of F≈0, 0.104⩽ L_o ⩽0.213 and 0.787 ⩽ T_t ⩽0.896 within the 0.236–0.248 [2$\pi c/a$] frequency range. The larger loss decreases T_t because some field energy leaks into the period layer between the two output waveguides from the MMI region. This loss can be reduced by adding a 180° arc waveguide with [n_2, h_2, r_0]=[4.6, 0.25a, a], where r_0 is the radius, as shown in Fig. 5(b).

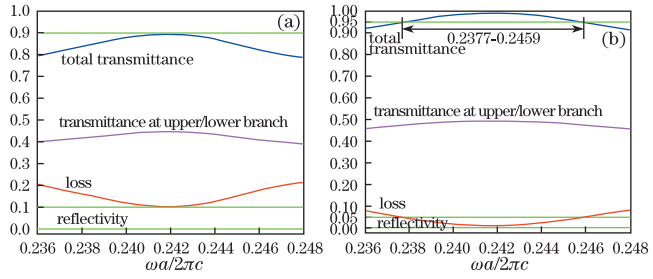

Fig. 6. (Color online) (a) Transmission characteristics of the 1×2 beam splitter with [h_{01}, h_{02}, L]=[3.75a, 9.75a, 10.4a] shown in Fig. 5(a); (b) transmission characteristics of the optimized 1×2 beam splitter with [h_{01},h_{02}, L, r_0]=[3.75a, 9.75a, 10.4a, a] shown in Fig. 5(b).

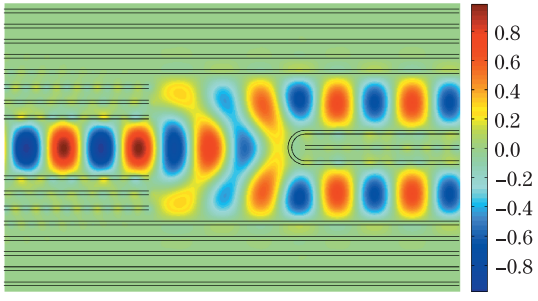

Fig. 7. (Color online) Steady-state electric field E_y distribution at the normalized frequency of 0.242[2$\pi c/a$] in the optimized 1×2 beam splitter shown in Fig. 5(b).

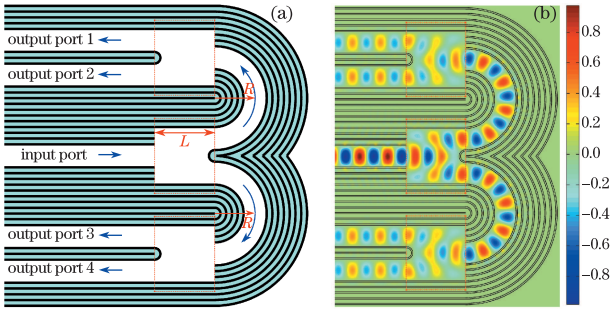

Fig. 8. (Color online) (a) Schematic drawing of the 1×4 beam splitter composed of three identical 1×2 beam splitters with [h_{01}, h_{02}, L, r_0] = [3.75a, 9.75a, 10.4a, a] and two groups of 180° arc flexible waveguides with curved radii R= 7a. (b) Steady-state electric field E_y distributions at the normalized frequency of 0.242 [2$\pi c/a$].

Figure 6(b) shows the transmission spectra, reflection spectrum, and loss spectrum of the optimized 1×2 beam splitters with [h_{01}, h_{02}, L,r_0]=[3.75a, 9.75a, 10.4a, a]. The optimized 1×2 beam splitter exhibited good transmission characteristics with a HTB of 0.2377–0.2459 [2$\pi c/a$], corresponding to the relative bandwidth of 3.39%. Figure 7 shows the steady-state electric field E_y distribution at the frequency 0.242 [2$\pi c/a$] in the optimized beam splitter.

Figure 8(a) shows the simple and compact 1×4 beam splitter that is constructed by combining the three optimized 1×2 beam splitters shown in Fig. 5(b) with the flexible bends of 1D PC waveguides. The 1×4 beam splitter consists of three identical 1×2 beam splitters, in which the middle beam splitter is defined as the first stage and the upper/lower beam splitter is defined as the second stage. The two stages were cascaded through two groups of 180° arc flexible waveguides, and the curvature radii of the two 180° arc flexible waveguides were set to 7a[12].

The incident light travels into the input port of the first-stage 1×2 beam splitter and is initially equally divided into two parts. The two parts are inputted into the two second-stage beam splitters through the 180° arc flexible waveguides and are then equally divided into two parts again. Finally, the incident light is equally divided into four parts through three 1×2 beam splitters.

The transmission characteristics of the 1×4 beam splitter were investigated using the FDTD method. The numerical results indicate that the frequency range of HTB is 0.2402–0.2438 [2$\pi c/a$]. The transmittances at the four output ports exhibited good consistencies. Figure 8(b) shows the steady-state electric field E_y distribution at the frequency of 0.242 [2$\pi c/a$] in the 1×4 beam splitter.

Finally, the presented beam splitters are notably compact. For example, when the optical communication wavelength of 1 550 nm was located at the frequency of 0.242 [2$\pi c/a$], the corresponding lattice constant a was 375 nm. When L_i=10a (L_i denotes the length of the straight waveguides on the input and output ports), the size of the fundamental 1×2 power splitter shown in Fig. 5(b) is approximately (30.4a×19a) 11.40×7.13 (μm) (with a HTB of 1 523–1 575 nm), while the total size of the 1×4 power splitter shown in Fig. 8(a) was approximately (36.95a×53a) 13.86×19.88 (μm) (with a HTB

of 1 539–1 562 nm). This size was two to three orders of magnitude less than the size currently used in optical stripe waveguides.

In conclusion, we present flexible optical waveguide beam splitters based on the self-imaging phenomena in multi-mode 1D PC waveguides. The beam splitters are simple, compact, and exhibit several advantages, such as high transmission, near-zero reflection, and low losses. The beam splitters in flattened form will be investigated in future studies, and they are expected to be applicable for use in highly dense photonic ICs.

This work was supported by the National Natural Science Foundation of China (No. 61007027) and the Fundamental Research Funds for Central Universities, China.

References

1. S. Fan, S. G. Johnson, J. D. Joannopoulos, C. Manolatou, and H. A. Haus, J. Opt. Soc. Am. B **18,** 162 (2001).
2. J. S. Jensen and O. Sigmund, J. Opt. Soc. Am. B **22,** 1191 (2005).
3. L. H. Frandsen, P. I. Borel, Y. X. Zhuang, A. Harpøth, M. Thorhauge, M. Kristensen, W. Bogaerts, P. Dumon, R. Baets, V. Wiaux, J. Wouters, and S. Beckx, Opt. Lett. **29,** 1623 (2004).
4. A. Têtu, M. Kristensen, LH Frandsen, A. Harpøth, P. I Borel, J. S. Jensen, and O. Sigmund, Opt. Express **13,** 8606 (2005).
5. A. Martinez, F. Cuesta, and J. Marti, IEEE Photon. Technol. Lett. **15,** 694 (2003).
6. I. Park, H. S. Lee, H. J. Kim, K. M. Moon, S. G. Lee, B.H. O, S. G. Park, and E. H. Lee, Opt. Express **12,** 3599 (2004).
7. A. Ghaffari, M. Djavid, and M. S. Abrishmian, Appl. Opt. **48,** 1606 (2009).
8. T. Liu, A. R. Zakharian, M. Fallahi, and M. Mansuripur, J. Lightwave Technol. **22,** 2842 (2004).
9. M. Zhang, R. Malureanu, A. C. Krüger, and M. Kristensen, Opt. Express **18,** 14944 (2010).
10. M. Zhang, A. C. Krüer, N. Groothoff, T. Balle, and M. Kristensen, Opt. Lett. **36,** 3058 (2011).
11. B. Chen, T. Tang, Z. Wang, H. Chen, and Z. Liu, Appl. Phys. Lett. **93,** 1811071 (2008).
12. B. Chen, T. Tang, and H. Chen, Opt. Express **17,** 5033 (2009).
13. B. Chen, L. Huang, Y. Li, C. Liu, and G. Liu, J. Opt. Soc. Am. B **28,** 2680 (2011).
14. S. G. Johnson and J. D. Joannopoulos, Opt. Express **8,** 173 (2001).
15. L. B. Soldano and E. C. M. Pennings, J. Lightwave Technol. **13,** 615 (1995).
16. A. Taflove and S. C. Hagness, *Computational Electrodynamics*: *The Finite-Difference Time Domain Method* (Artech House, Boston, 2000).